Development of 150000 r/min, 1.5 kW Permanent-Magnet Motor for Automotive Supercharger

Toshihiko Noguchi [*], *IEEE Senior Member*, and Masaru Kano [*]

[*] Nagaoka University of Technology
Address: 1603-1 Kamitomioka, Nagaoka, Niigata 940-2188, Japan
Phone: +81-258-47-9510, Fax: +81-258-47-9500
e-mail: tnoguchi@vos.nagaokaut.ac.jp

***Abstract*—This paper discusses an optimum design of an ultra high-speed permanent-magnet synchronous motor (PMSM), which is applied to a supercharger of an automotive engine. Although the motor is driven by an inverter with a 12-V DC bus voltage due to an automotive power source, it achieves the maximum rotating speed of 150000 r/min and the rated output of 1.5 kW. Since the power source strictly restricts the motor terminal voltages and the fundamental operating frequency is as high as 2500 Hz, it is significant to pursue further reduction of the synchronous impedance in the motor, paying attention to its permeance coefficient. In the paper, a FEM-based electromagnetic field analysis is conducted, followed by a theoretical discussion on the optimum machine design. In addition, the mechanical structure is discussed to produce a real machine. The developed prototype has a variety of unique features from electrical and mechanical viewpoints, and some experimental test results are presented to demonstrate its potential.**

***Index Terms*— ultra high-speed, permanent-magnet synchronous motor, supercharger, electromagnetic field analysis, and permeance coefficient.**

I. Introduction

Superchargers are often used on automotive combustion engines to enhance the engine output power and to reduce the physical engine size at the same time. Not only the performance improvement in a power-weight ratio of the engines but also various advantages over common power plants can be expected, such as a quality improvement of the exhaust gas, a fuel-efficiency improvement with respect to the output power, and a quick response of the engine torque. A conventional supercharger has a mechanical linkage with the engine, which uses a timing belt from the crankshaft via overdrive devices, and it compresses inlet air to the engine cylinders by means of the mechanical power provided by the engine. Fig. 1 illustrates a mechanical configuration of the traditional supercharging system. As shown here, many of such conventional superchargers employ a positive displacement compressor rather than a centrifugal compressor because of limitation of the operating speed due to the low engine-rotation. Low-efficiency and low boost-pressure are, however, major drawbacks of the positive displacement compressor, which prevents further performance improvement of the supercharged engines.

On the other hand, an electrical drive of the supercharger is a very promising approach as a next-generation axulially machine in future automobiles. Fig. 2 depicts an outline of the investigated supercharging system for the automotive combustion engines. Since the electrically driven supercharger allows to employ the centrifugal compressor instead of the positive displacement compressor, highly efficient operation can be achieved, e.g., higher operating speed over 100000 r/min, higher boost-pressure, smaller mechanical dimensions, faster response of the inlet air compression, etc. Furthermore, there is another advantage of the electric supercharger in a mechanical-linkage-free structure, which reduces overall mechanical losses and eliminates complicated link mechanism.

This paper discusses an optimum design of an ultra high-speed permanent-magnet synchronous motor (PMSM), which is specifically applied to the electric supercharger of the automotive engines. Although the PMSM is operated by an inverter with a 12-V DC bus voltage for an adjustable-speed drive, it must attain the maximum rotating speed of 150000 r/min and the rated output power of 1.5 kW for electrification of the centrifugal-compressor-based supercharger. There are various difficult technical problems in the machine

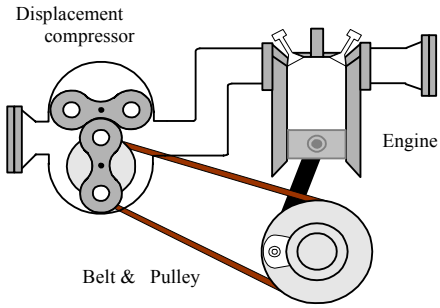

Fig. 1. System configuration of conventional supercharging system.

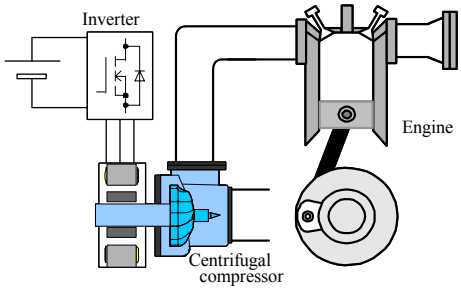

Fig. 2. System configuration of electric supercharging system.

TABLE I. Target specifications of ultra high-speed motor.

Assumed engine	1.5 L class
Rated output power	1.5 kW
Rated speed	150000 r/min
Rated torque	0.0955 Nm
Overload capacity and duration	200 %, 1 s

TABLE II. Electrical and mechanical design parameters of ultra high-speed motor.

Rated voltage	2.96 V/phase
Rated current	195 A
Number of phases	3 phase
Number of poles	2 poles
Stator configuration	Concentrated winding structure
Winding configuration	1 turn, 2 parallels per phase
Number of stator slots	6 slots
Stator outer diameter	92 mm
Stator inner diameter	28 mm
Stator stack length	30 mm
Stator tooth width	10 mm
Electromagnetic steel plates	10JNEX900 (0.1-mm thick, 6.5-% silicone, μ_s=23, B_{max}=1.8 T)
Rotor shaft diameter	12 mm
Permanent magnet	N-42SH Nd-Fe-B (Br=1.28 T, bHc=955 kA/m, BH_{max}=310 kJ/m^3)
Bearings	Angular ceramic-ball bearing with grease lubrication

design, e.g., drastic reduction of the synchronous impedance, minimization of the iron and the copper losses, further improvement of the power-weight ratio, etc., which should simultaneously be solved with compromise to some extent. In addition, these electrical design requirements must be satisfied all together with a compact and robust mechanical structure design. In the design process, a finite-element-method (FEM)-based electromagnetic field analysis is conducted to make the fine adjustment of the detailed machine shape and to seek the best design parameter set, focusing on a permeance coefficient of the PMSM. The mechanical structure is also discussed to create a real prototype machine, which is experimentally examined to confirm the basic performance as a first step of the system development.

II. Requirements and Design Specifications for Ultra High-Speed Motor

A. Requirements for Ultra High-Speed Motor

Assuming that the centrifugal compressor is employed for a supercharger mounted on a 1.5-litter class gasoline engine, the ultra high-speed motor is required to output the mechanical power from 1.5 to 2 kW at 150000 r/min or higher. Particularly, when boosting the inlet air compression, extremely fast response is indispensable to accelerate the compressor from several thousand r/min to the rated operating speed of 150000 r/min within approximately 0.5 s, which is almost comparable with a response time of the conventional supercharger. In order to meet with this requirement, the ultra high-speed motor must have an overload capacity double of the rated output power at least for one second. Taking these requirements for the motor into account, the target specifications are determined as listed in TABLE I.

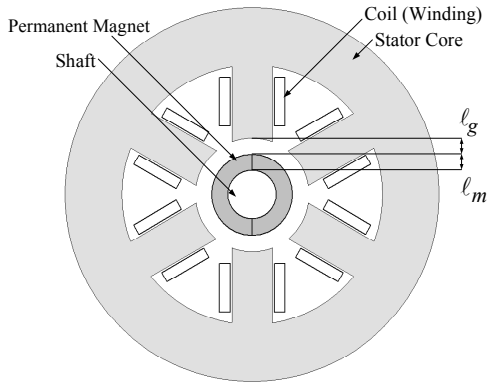

Fig. 3. Cross section diagram of ultra high-speed SPMSM.

TABLE III. Design conditions of five different permeance coefficients.

Design type	#1	#2	#3	#4	#5
Air gap length ℓ_g (mm)	6	5	4	3	2
Permanent magnet thickness ℓ_m (mm)	2	3	4	5	6
Permeance coefficient	0.33	0.6	1	1.67	3

B. Basic Design Concept of Ultra High-Speed Motor

On the basis of the target specifications, detailed electrical and mechanical design parameters must be investigated prior to the numerical analysis for the best solution. In order to achieve the highest efficiency among various electric machines, a two-pole three-phase surface permanent-magnet synchronous motor (SPMSM) is selected as the best rotating machine for the ultra high-speed motor drive because of no magnetizing current required unlike an induction motor or a reluctance motor. A strong Nd-Fe-B permanent magnet of the rotor allows not only improvement of the motor efficiency but also drastic size reduction of the rotor to restrict its circumference speed and to mitigate the centrifugal force effect, which is of vital importance in the ultra high-speed motor. Using such powerful Nd-Fe-B permanent magnet that has 310-kJ/m^3 BH_{max} makes a wide-air-gap design possible to reduce the synchronous reactance and to obtain a sinusoidal electromotive force (e.m.f.) regardless of the concentrated stator winding structure.

On the other hand, the stator has a six-teeth and six-slot structure and the concentrated windings because the motor is required to reduce the leakage inductance thoroughly as well as the synchronous reactance. It should be noted that each phase has a pair of single-turn windings in parallel. The stator core must be designed to have as low iron-losses as possible even at 150000 r/min. Therefore, high-performance 6.5-% silicone electromagnetic steel plates of which thickness is only 0.1 mm are employed to compose the laminated stator iron core. TABLE II is a summary of the basic conceptual design for the ultra high-speed SPMSM to be investigated in the paper.

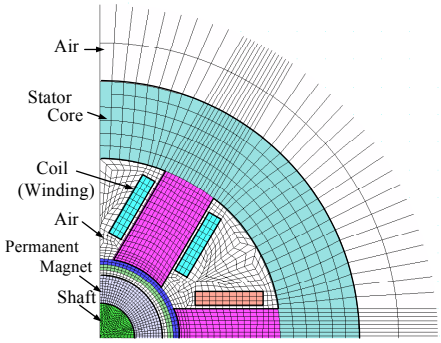

Fig. 4. Generated mesh for FEM analysis only in quarter portion.

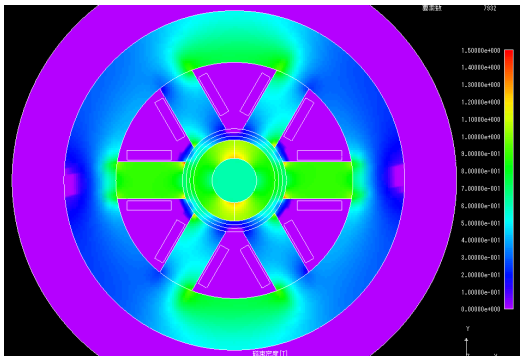

Fig. 5. Example of flux density distribution at rated operation.

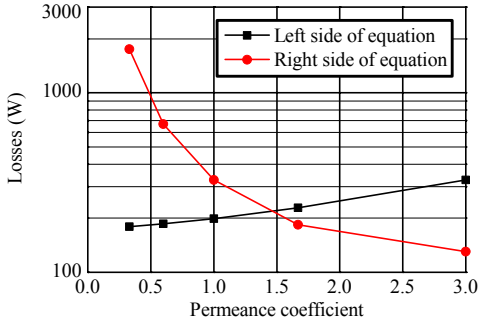

Fig. 6. Loss characteristics with respect to permeance coefficient.

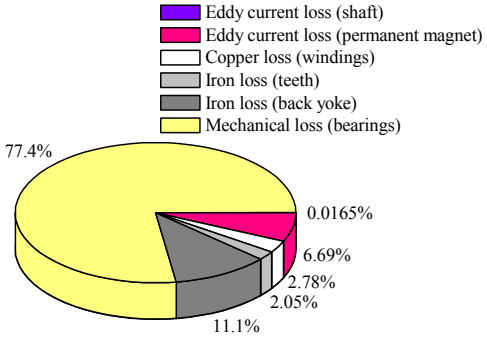

Fig. 7. Numerically calculated losses of design type #4.

III. Theoretical Discussion and Electromagnetic Field Analysis for Optimum Motor Design

A. Theoretical Discussion for Optimum Motor Design

It is well known that the operation characteristics of the SPMSM dominantly depend on the permeance coefficient because it determines an operating point of the permanent magnet on its B-H curve. Assuming that the investigated SPMSM has uniform permeance distribution along the air gap, the permeance coefficient p_u of the SPMSM is expressed by the following equation:

$$p_u = \frac{\ell_m}{a_m}\frac{a_g}{K_C \ell_g} = \frac{\ell_m}{D_m - \ell_m}\frac{D_m + \ell_g}{K_C \ell_g}, \quad (1)$$

where ℓ_m is a permanent-magnet thickness, a_m is an averaged cross sectional area of the permanent magnet, a_g is an averaged cross sectional area of the air gap between the rotor and the stator, ℓ_g is an air gap length, D_m is an outer diameter of the permanent magnet, and K_C is a Carter's coefficient. Since K_C normally takes a value of approximately 1.2 to 1.5, a_g can be regarded as almost same as $a_m K_C$; thus, the following approximated expression is obtained:

$$p_u \approx \frac{\ell_m}{\ell_g}. \quad (2)$$

This equation indicates that the permeance coefficient is determined by the ratio between ℓ_m and ℓ_g as illustrated in Fig. 3. The permeance coefficient p_u is basically proportional to the e.m.f. if other physical dimensions of the investigated motor are not changed.

On the other hand, in order to improve the total efficiency of the motor drive system including the inverter, the inverter loss must be taken into account. The maximum efficiency condition of the motor drive system can be expressed as

$$W_i^{st} + W_e^{mag} + W_m = W_c + W_{Ron}, \quad (3)$$

where W_i^{st} is an iron loss of the stator core, W_e^{mag} is an eddy-current loss of the permanent magnet, W_m is a mechanical loss (bearing friction loss), W_c is a copper loss of the stator windings, and W_{Ron} is a conduction loss of the inverter. The left-hand side terms of (3) are not contingent upon the line currents of the motor, while the right-hand side terms are almost proportional to square of the currents. There is a switching loss as well as the conduction loss in the inverter, but the switching loss does not affect the maximum efficiency condition indicated by (3) because it is proportional to the line currents.

B. FEM-Based Electromagnetic Analysis and Results

TABLE III shows analytical conditions of the ultra high-speed SPMSM, where five combinations of the permeance coefficient, i.e., the permanent-magnet thickness ℓ_m and the air gap length ℓ_g, are investigated. Figs. 4 and 5 are a quarter portion of the generated mesh (7692 elements and 7909 nodes in the whole mesh) and an example of the resultant magnetic-flux density distribution, respectively. As shown in this example, the mean value of the flux density is approximately 0.45 T in the air gap, while significant magnetic saturation is hardly observed in the iron core. Fig. 6 shows the loss analysis result, where the left-hand side terms and the right-hand side terms in (3) are separately drawn with respect to p_u. It can be found from this figure that (3) is satisfied at p_u = 1.5, i.e., the total loss is minimized at this

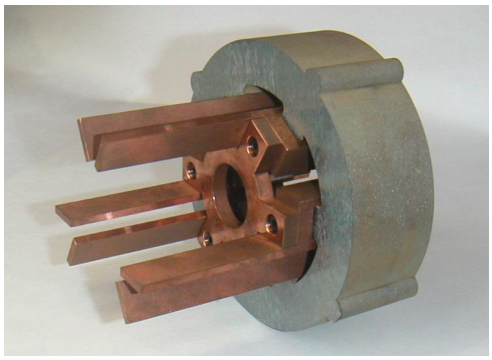

(a) Stator core made of 0.1-mm thick, 6.5-% silicone electromagnetic steel plates and single-turn stator windings.

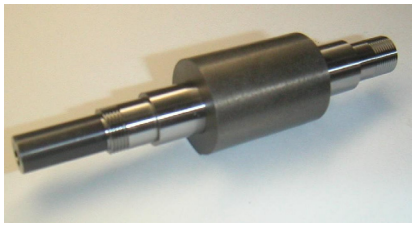

(b) Nd-Fe-B permanent-magnet rotor before mechanical reinforcement using carbon fiber.
Fig. 8. Photographs of stator and rotor.

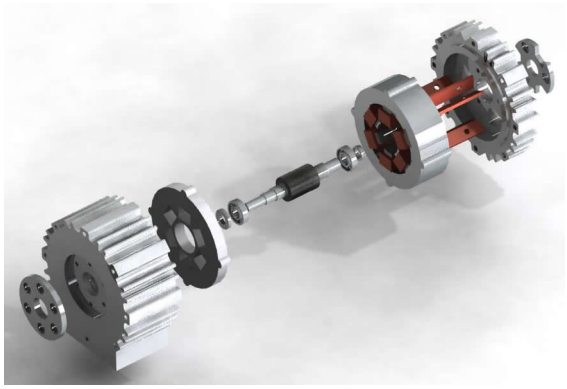

Fig. 9. Three-dimensional computer graphic of motor assembly.

condition. Therefore, the design type of #4 (ℓ_m = 5 mm and ℓ_g = 3 mm), which has the nearest permeance coefficient to p_u = 1.5, is introduced to the prototype machine production. Fig. 7 represents numerically calculated losses of the design type #4. As can be seen in the figure, the mechanical friction loss is dominant, which accounts for 77.4 %, while the stator iron loss and the eddy-current loss on the permanent magnet are merely 19.8 % of the total loss. The electrical efficiency except for the mechanical loss is approximately 95 %.

IV. Electrical and Mechanical Structure of Prototype Machine

As described in the basic design concept of the ultra high-speed motor, the prototype has a special electrical and mechanical structure. Fig. 8 shows photographs of the stator and the rotor. The laminated stator core consists of approximately 300 sheets of 6.5-% silicone electromagnetic steel plates, of which outer diameter is 92 mm, inner diameter is 28 mm, and axially stack length

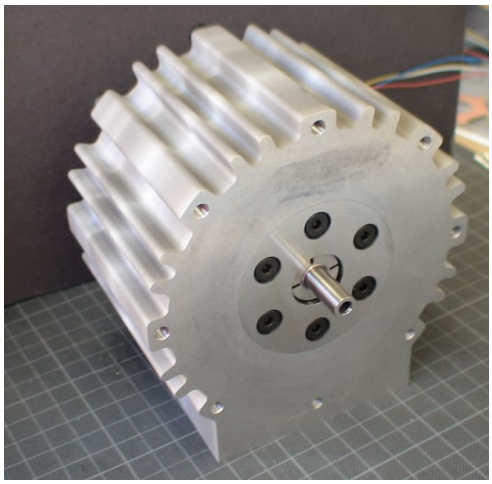

(a) Front view (load side) of prototype machine.

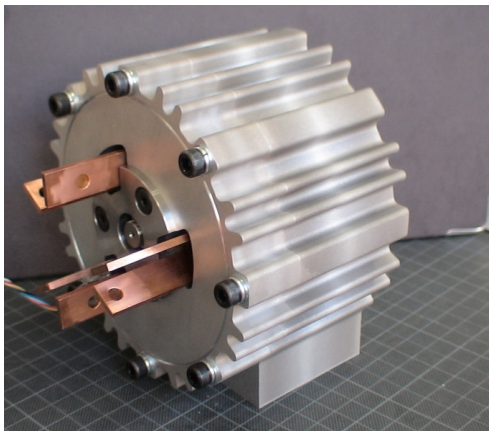

(b) Rear view (opposite side of load) of prototype machine.
Fig. 10. Exterior photographs of prototype machine.

is 30 mm. An alphabetically "b"-shaped stator-winding bar is inserted in each stator tooth with keeping electrical insulation from the stator core by polyimide taping, and is connected to a neutral-point end ring together with the other stator windings. Each of the stator windings has cross sectional area of 31.2 mm^2, resulting in current density of approximately 6.25 A/mm^2 at rated load. Every clearance between the tooth and the stator winding is less than 0.5 mm, which effectively improves the magnetic coupling by reducing the leakage inductance. On the other hand, the rotor is simply assembled with a steel shaft and the ring-shaped Nd-Fe-B permanent magnet, and is magnetized so that the flux distribution becomes sinusoidal. The photograph of the rotor shows exterior of the permanent magnet before mechanical reinforcement with carbon fiber. After assembling the rotor, 1.5-mm thick layer of the carbon fiber is formed with special epoxy resin on the permanent magnet surface against large centrifugal force. Fig. 9 illustrates a three-dimensional computer graphic (a bird's-eye view) of the prototype motor assembly. All of the metal components are made with highly precise NC machining tools. Particularly, bearings are the most important parts to realize the ultra high-speed operation. In the real machine, a pair of super-precise angular ceramic ball bearings is used because the prototype is just

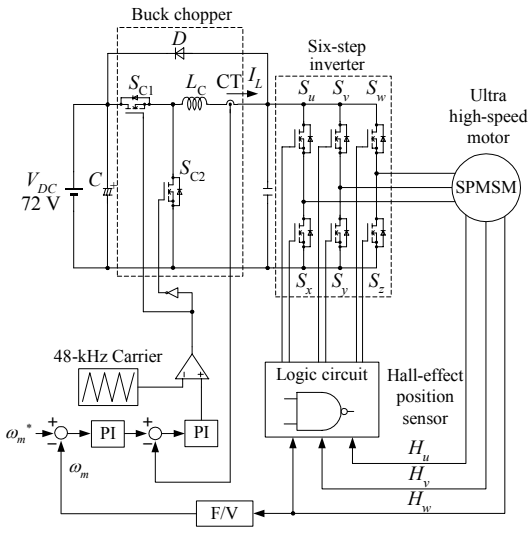

Fig. 11. Schematic diagram of pseudo current-source inverter drive.

TABLE IV. Measurement result of motor parameters.

Motor parameters	Designed value	Measured value
E.m.f constant (10^{-5} V/r/min)	1.96	1.89
R_a (mΩ)	0.054	0.072
L_a (μH)	0.056	0.07

experimentally examined and requires neither high reliability nor mechanical endurance in the laboratory tests. However, the prototype is designed and created to have extremely high accuracy of μm-order, especially in the bearing and shaft part. Fig. 10 shows a front view and a rear view of the assembled prototype motor.

V. Experimental System and Test Results

A prototype motor was tested to confirm several basic operation characteristics with an experimental setup illustrated in Fig. 11. Since the fundamental operating frequency of the test motor is over 2 kHz, a pseudo current-source inverter was employed to drive the motor instead of a common voltage-source PWM inverter. The pseudo current-source inverter features a current-controlled buck chopper part and a six-step inverter part. The former has a DC bus current feedback loop and controls the DC bus current in accordance with a torque command coming from a speed control loop. Therefore, it can be regarded as a regulated current-source, which achieves PAM of the DC bus current. This approach is superior to ordinary thyristor-based power converters because it operates at the switching frequency of 48 kHz, resulting in drastic reduction of the DC bus inductance and in millisecond-order fast response of the DC bus current control. On the other hand, the six-step inverter commutates the DC bus current, and generates 120-deg conduction patterns of the line currents. Every time the current is commutated, the synchronous inductance of the motor and the line inductance generate surge voltages across the inverter terminals. In the case of the pseudo current source inverter, however, the DC bus voltage clamps the surge voltages via body-diodes in the inverter MOSFETs and a bypass diode of the buck chopper. The

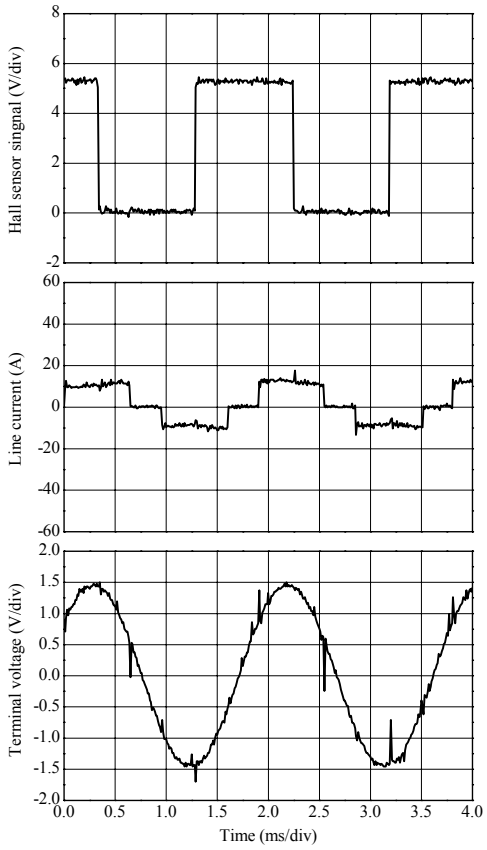

Fig. 12. Operating waveforms at 33000 r/min under no-load condition.

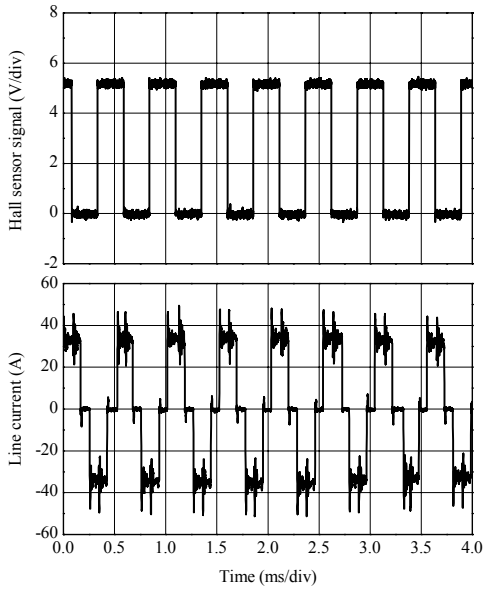

Fig. 13. Operating waveforms at 120000 r/min under no-load condition.

current commutation is controlled by a logic circuit where three-phase Hall-effect sensor signals generate the 120-deg conduction patterns.

TABLE IV indicates comparison between the designed and the experimentally measured motor parameters. As listed here, both of the winding resistance and the inductance of the real machine are slightly higher than the designed values. It is inferred that the higher resistance is due to contact resistance between the winding bars and

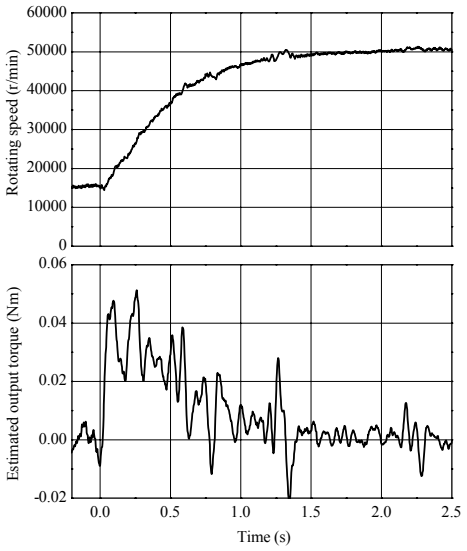

Fig. 14. Speed step response from 15000 to 50000 r/min and experimentally estimated output torque.

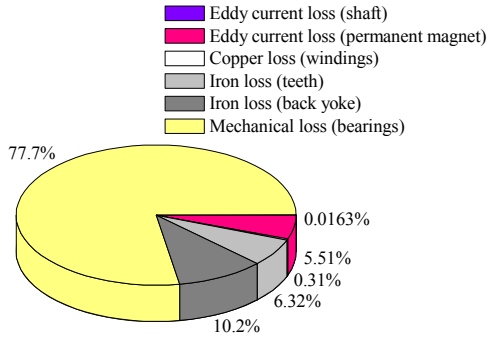

Fig. 15. Experimentally estimated loss-analysis result.

the neutral-point end ring and that the higher inductance includes line inductance and the leakage inductance.

Fig. 12 shows waveforms of the Hall-effect position sensor signal, a line current and a motor terminal voltage, which were measured at approximately 33000 r/min in a test run. The current has low amplitude of approximately 10 A because of no-load operation, and its 120-deg conduction pattern is generated synchronously with the output signal of the Hall-effect position sensor. Since the motor terminal voltage is sinusoidal without conspicuous harmonic distortion, which means the e.m.f. is properly generated by the permanent magnet on the rotor in spite of the concentrated winding structure of the stator. Fig. 13 demonstrates operating waveforms of the prototype at 120000 r/min under no-load condition. As can be seen in the figure, an excellent current waveform with 120-deg conduction pattern is properly obtained, which is in phase with the Hall-effect position sensor signal.

In addition, an acceleration test was conducted to check the output-torque controllability. In general, it is rather difficult to measure the mechanical output at such an ultra high-speed as 150000 r/min, so the output torque of the test motor was estimated by acceleration in the speed step response waveform and a design value of the rotor inertia. From Fig. 14, it is inferred that the maximum output torque in the acceleration from 15000 to 50000 r/min is 0.05 Nm, which is half of the rated value. Although the output torque waveform is quite choppy as indicated in Fig. 14, it can be found from the waveform envelope that the PI regulator in the speed loop linearly controls the torque.

Fig. 15 shows an experimentally estimated loss analysis result. There can be seen a good agreement with the numerically analyzed result shown in Fig. 7 in the overall loss percentage, where the mechanical friction loss caused by the bearings is dominant and the stator iron losses and the eddy-current loss of the permanent magnet account for 22.0 % of the total loss.

VI. Conclusion

This paper described development of an ultra high-speed SPMSM, of which ratings are 150000 r/min and 1.5 kW. The prototype has various unique features from electrical and mechanical viewpoints to realize the ultra high-speed drive fed by a 12-V DC power source like batteries. A 120000-r/min operation under no-load condition and speed step response to 50000 r/min were examined, and proper operation characteristics were confirmed through some experimental tests. Furthermore, experimentally estimated loss analysis result agreed very well with the FEM-based electromagnetic field analysis result. Consequently, the dominant loss factor was found to be a mechanical loss dissipated by the bearings.

References

[1] M. Okawa, "Design Manual of Magnetic Circuit and PM Motor," *Sogo Research*, 1989 (in Japanese).

[2] T. Koganezawa, I. Takahashi, and K. Ohyama, "Sensorless Speed Control of a PM Motor by a Quasi-Current Source Inverter," *IEE-Japan Proc. of Ind. App. Soc. Ann. Conf.*, p. 175, 1992 (in Japanese).

[3] I. Takahashi, T. Koganezawa, T. Su G., and K. Ohyama, "A Super High Speed PM Motor Drive System by a Quasi-Current Source Inverter." *IEEE Trans. on Ind. App.*, vol. 30, no. 3, p.p. 683-690, 1994.

[4] B. –H. Bae, and S. –K. Sul, "A Compensation Method for Time Delay of Full-Digital Synchronous Frame Current Regulator of PWM AC Drives," *IEEE Trans. on Ind. App.*, vol. 39, no. 3, p.p. 802-810, 2003.

[5] B. –H. Bae, S. –K. Sul, J. –H. Kwon, and J. –S. Byeon, "Implementation of Sensorless Vector Control for Super-High-Speed PMSM of Turbo-Compressor," *IEEE Trans. on Ind. App.*, vol. 39, no. 3, p.p. 811-818, 2003.

[6] T. Noguchi, Y. Takata, Y. Yamashita, Y. Komatsu, and S. Ibaraki, "220000r/min, 2-kW Permanent Magnet Motor Drive for Turbocharger", *IEE-Japan Int. Power Elec. Conf. (IPEC) -Niigata*, p.p. 2280-2285, 2005.

[7] T. Noguchi, Y. Takata, Y. Yamashita, Y. Komatsu, and S. Ibaraki, "220000r/min, 2-kW PM Motor Drive for Turbocharger", *IEE-Japan Trans. on Ind. App.*, vol. 125, no. 9, p.p. 854-861, 2005 (in Japanese).

[8] T. Noguchi, Y. Takata, Y. Yamashita, and S. Ibaraki, "160,000-r/min 2.7-kW Electric Drive of Supercharger for Automobiles." *The Sixth Int. Conf. on Power Elec. and Drive Sys. (PEDS) –Kuala Lumpur*, p.p. 1380-1385, 2005.

[9] C. Zwyssig, M. Duerr, D. Hassler, and J. W. Kolar, "An Ultra-High-Speed, 500000 rpm, 1 kW Electrical Drive System," *The Fourth Power Conv. Conf. (PCC) –Nagoya*, CDROM, 2007.